

Engineered holo cytochrome *c* synthases that biosynthesize new cytochromes *c*

Deanna L. Mendez^a, Shalon E. Babbitt^a, Jeremy D. King^a, John D'Alessandro^a, Michael B. Watson^b, Robert E. Blankenship^a, Liviu M. Mirica^b, and Robert G. Kranz^{a,1}

^aDepartment of Biology, Washington University in St. Louis, St. Louis, MO 63130; and ^bDepartment of Chemistry, Washington University in St. Louis, St. Louis, MO 63130

Edited by Robert Haselkorn, University of Chicago, Chicago, IL, and approved January 20, 2017 (received for review September 27, 2016)

Cytochrome *c* (cyt *c*), required for electron transport in mitochondria, possesses a covalently attached heme cofactor. Attachment is catalyzed by holo cytochrome *c* synthase (HCCS), leading to two thioether bonds between heme and a conserved CXXCH motif of cyt *c*. In cyt *c*, histidine (His19) of CXXCH acts as an axial ligand to heme iron and upon release of holo cytochrome *c* from HCCS, folding leads to formation of a second axial interaction with methionine (Met81). We previously discovered mutations in human HCCS that facilitate increased biosynthesis of cyt *c* in recombinant *Escherichia coli*. Focusing on HCCS E159A, novel cyt *c* variants in quantities that are sufficient for biophysical analysis are biosynthesized. Cyt *c* H19M, the first bis-Met liganded cyt *c*, is compared with other axial ligand variants (M81A, M81H) and single thioether cyt *c* variants. For variants with axial ligand substitutions, electronic absorption, near-UV circular dichroism, and electron paramagnetic resonance spectroscopy provide evidence that axial ligands are changed and the heme environment is altered. Circular dichroism spectra in far UV and thermal denaturation analyses demonstrate that axial ligand changes do not affect secondary structures and stability. Redox potentials span a 400-mV range (+349 mV vs. standard hydrogen electrode, H19M; +252 mV, WT; -19 mV, M81A; -69 mV, M81H). We discuss the results in the context of a four-step mechanism for HCCS, whereby HCCS mutants such as E159A are enhanced in release (step 4) of cyt *c* from the HCCS active site; thus, we term these "release mutants."

cytochrome *c* | HCCS | heme | spectroscopy | axial ligands

The mitochondrial monoheme cytochrome *c* (cyt *c*) is one of the most studied proteins with respect to its structure, function, and folding. Cyt *c* is unique because it possesses two covalent thioether bonds between the vinyl groups of heme and two thiols of the protein, at a conserved CXXCH motif. The histidine of CXXCH acts as an axial ligand to heme iron in all cyt *c* proteins. Thioether attachment is catalyzed by a single enzyme called holo cytochrome *c* synthase (HCCS), which functions in the mitochondrial intermembrane space (1, 2). Results from biochemical studies on human HCCS and cyt *c*, functionally expressed in recombinant *Escherichia coli*, have led to the proposal of a four-step model for biosynthesis by HCCS (Fig. 1) (3–6). Step 1 entails the binding of heme; certain HCCS mutants are defective in this step (5), including the E159K substitution that is responsible for microphthalmia with linear skin syndrome (MLS) (HCCS sequence in Fig. S1A, numbering from human HCCS). Another HCCS mutant in step 1, H154A, is unable to bind heme, but is corrected for in vivo function by exogenous imidazole (4). Spectroscopy and mutagenesis studies also established HCCS His154 as an axial ligand for heme binding. In step 2, apo cyt *c* binds to holo HCCS, with histidine (His-19) of CXXCH providing the second axial ligand in this complex (6). Step 3 is formation of the two thioether bonds, which distorts the heme, weakening interaction with the HCCS (6). This distortion in part promotes step 4, release of holo cyt *c* from HCCS, before cyt *c* folding. A previous study by Babbitt et al. has speculated that certain HCCS substitutions affect release step 4 (Fig. 1) (5). These HCCS mutants appear to enhance release of cyt *c*, biosynthesizing 1.5- to 2-fold more cyt *c* (than WT HCCS), and they also copurify with less cyt *c* than the WT HCCS.

Thus, these are lower in steady-state levels of HCCS/cyt *c* complex (Fig. 1, steps 2 and 3) but yield higher levels of released and folded cyt *c* product.

Evidence suggests there is a balance in requirements for heme binding by HCCS in step 1 and need for heme release in step 4 (as holo cyt *c*). Studies on HCCS E159 substitutions, the MLS residue, provide some of this evidence (5). An HCCS E159K substitution is defective in step 1 and results in reduced cyt *c* biosynthesis in recombinant *E. coli*, whereas HCCS E159A enhances biosynthesis. Both HCCS E159K and E159A purify with less endogenous heme than wt HCCS and when coexpressed with human cyt *c*, copurify with less holo cyt *c*. Moreover, certain HCCS mutants that are defective in step 1, including E159K and W162A, are corrected for function (i.e., cyt *c* biosynthesis) in recombinant *E. coli* by exogenous aminolevulinic acid, which increases heme synthesis (5). These data support the proposal that HCCS Glu159 and Trp162 are involved in heme binding and that a balance in heme levels (in vivo), heme binding and release by HCCS all impact holo-cyt *c* biosynthesis.

Saccharomyces cerevisiae HCCS has been used in recombinant *E. coli* previously to biosynthesize WT cyt *c* and selected cyt *c* variants, such as single thioether (e.g., SXXCH), M81A, and a few other cyt *c*s (7–9). However, HCCS does not appear to recognize (or at least biosynthesize) single thioether variants where the second cysteine is substituted (e.g., CXXSH) (7). Histidine ligand variants (e.g., CXXCM, bis-Met) have also not been produced, nor does bis-Met or single thioether (CXXXH) exist in nature. In this study, we use human HCCS mutants to show that they release and biosynthesize certain cyt *c* variants at higher levels than WT HCCS, including a bis-Met cyt *c*. Results support the proposal that such engineered HCCS mutants are involved in the release step 4. We speculate that weakening the interaction of heme in these HCCS mutants (step 4)

Significance

Specific mutations in human holo cytochrome *c* synthase (HCCS) confer enhanced biosynthesis of cyt *c*, including cyt *c* variants never before produced. These include a bis-Met and single thioether cyt *c*. We designate these as HCCS "release mutants" because evidence indicates they are mechanistically affected in step 4 of biosynthesis, release of cyt *c* from the HCCS/cyt *c* complex. Characteristics of cyt *c* WT (His/Met), cyt *c* H19M (bis-Met), cyt *c* M81H (bis-His), and cyt *c* M81A (His/OH⁻) indicate proper folding and that the engineered ligands are present. This panel of variants spans a redox gradient of more than 400 mV, which will be useful for studying various redox-dependent cellular processes and other physical properties.

Author contributions: D.L.M. and R.G.K. designed research; D.L.M., J.D.K., J.D., and M.B.W. performed research; S.E.B. and L.M.M. contributed new reagents/analytic tools; S.E.B., J.D.K., R.E.B., L.M.M., and R.G.K. analyzed data; and D.L.M., L.M.M., and R.G.K. wrote the paper.

The authors declare no conflict of interest.

This article is a PNAS Direct Submission.

¹To whom correspondence should be addressed. Email: kranz@wustl.edu.

This article contains supporting information online at www.pnas.org/lookup/suppl/doi:10.1073/pnas.1615929114/-DCSupplemental.

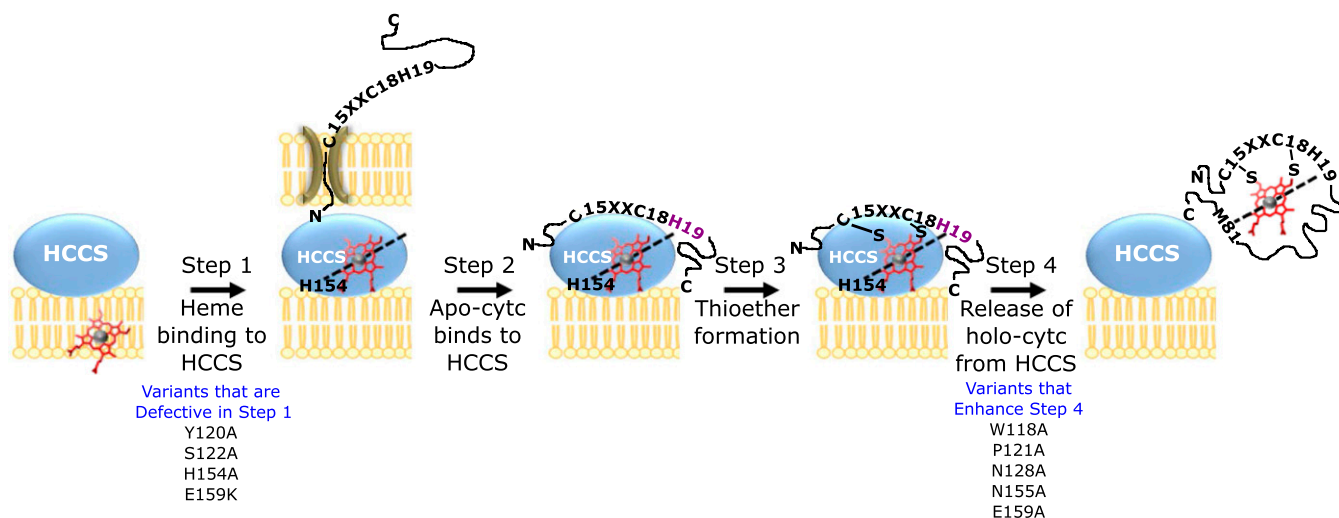


Fig. 1. HCCS model for cytochrome *c* assembly. Classifiable mutants are listed below the step in which they are defective or enhanced.

facilitates release of the cytochrome *c* variants from the HCCS enzyme, which resets HCCS for further catalysis (step 1).

Results

Use of HCCS Mutants to Biosynthesize cytochrome *c* Variants. Certain HCCS mutants biosynthesize WT cytochrome *c* at modestly higher levels (1.5- to 2-fold) than WT HCCS (5). We initially chose two cytochrome *c* variants never before biosynthesized that are poorly expressed by WT HCCS, to determine if higher levels could be biosynthesized using selected HCCS mutants (HCCS_E159A, HCCS_N155A, HCCS_W118A). This included the human cytochrome *c* bis-Met variant, H19M, and the second thioether variant, C18A. The human cytochrome *c* sequence is shown in Fig. S1B (numbering includes initiator methionine). For these preliminary studies, nonhexahistidine-tagged cytochrome *c* variants were used. Cytochrome *c* variants were induced with 0.16% arabinose and HCCS W118A, N155A, or E159A with isopropyl- β -D-thiogalactopyranoside (IPTG) in *E. coli* deleted of its own cytochrome *c* biogenesis pathway (MG1655 Δ ccm) (10). Cytochrome *c* levels were quantified from 1-L culture supernatants after ion exchange chromatography. For cytochrome *c* H19M, HCCS W118A biosynthesized twofold, N155A threefold, and E159A ninefold higher levels than WT HCCS. For the cytochrome *c* C18A variant, HCCS W118A yielded 6-fold, N155A 3-fold, and E159A greater than 10-fold higher levels compared with WT HCCS.

We focused on HCCS E159A, constructing a variety of cytochrome *c* variants to test, many containing cleavable hexahistidine tags for further purification and analyses. Cytochrome *c* variants included both axial ligand and thioether substitutions (Table S1). These studies confirmed initial results with the overproduction of cytochrome *c* H19M and C18A, in addition to the C18S variant. We chose to analyze cytochrome *c* axial ligand variants in detail because a bis-Met cytochrome *c* has never been made, thus facilitating a comparison in changes to both axial ligands. Mass spectrometry analyses of intact WT (12,365 Da) had the most abundant peak at $12,232 \pm 5$ ppm, and the H19M cytochrome *c* (12,359 Da) had the most-abundant peak at $12,226 \pm 5$ ppm. The difference between the calculated values for intact cytochrome *c* and cytochrome *c* H19M and the measured values is 133 Da, consistent with the cleavage of the initiating Met (131 Da). The 2-Da difference is within the experimental error (Fig. S2). The size difference between cytochrome *c* WT and H19M is that of a His/Met substitution with heme covalently attached in both cytochrome *c* proteins and no other modifications. We overexpressed and purified four cytochrome *c* proteins with cleavable hexahistidine tags and putative axial ligand changes (WT = His/Met, H19M = Met/Met, M81A = His/none, M81H = His/His). Proteins were purified by

ion exchange and cobalt column chromatography. The proteins were pure as determined by SDS/PAGE (Fig. S3) and all were monomeric as determined by gel-filtration HPLC (Fig. S4).

UV-vis Spectroscopy of cytochrome *c* Axial Ligand Variants. Human cytochrome *c* showed typical characteristics by UV-vis spectroscopy (Fig. 2A), including a 549.5-nm α -peak in the reduced (Fe^{2+}) state and a red shift of the Soret peak upon reduction. The inset in Fig. 2A of the ferric cytochrome *c* shows the weak 695-nm band characteristic of the Met ligation. Table S2 shows the peak absorptions observed here compared with those reported in the literature. The spectrum of cytochrome *c* M81H (bis-His) was very similar to cytochrome *c* (Fig. 2B) with the exception that the 695-nm band is absent in the ferric species. To our knowledge, no biosynthesized cytochrome *c* M81H variants have been reported, although a chemically synthesized horse heart cytochrome *c* M81H exhibits similar spectra (11). Cytochrome *c* M81A spectra (Fig. 2C) show only minor differences between oxidized and reduced forms, with no sharp α - or β -peaks in the reduced state, and a small red shift (3–5 nm) of the Soret upon reduction. The ferrous cytochrome *c* M81A biosynthesized here has a Soret peak at 411 nm with a

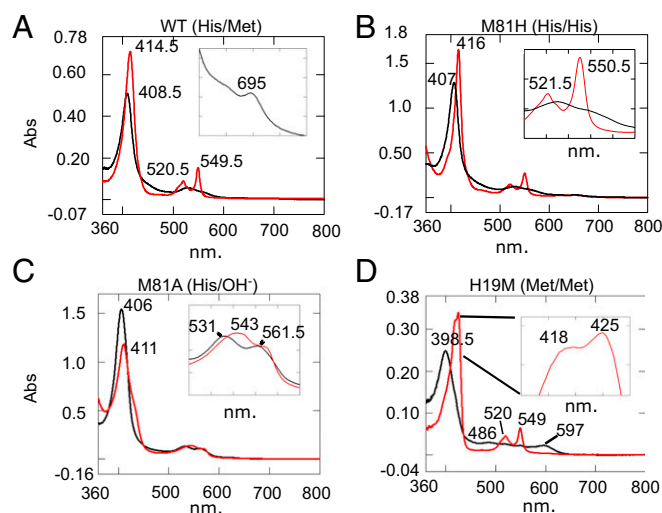


Fig. 2. UV-vis spectra of cytochromes *c*: WT (A), bis-His (M81H) (B), mono-His (M81A) (C), and bis-Met (H19M) (D). The reduced spectra are shown in red and the oxidized spectra are shown in black.

shoulder at 434 nm, a peak at 544 nm with a shoulder at 563 nm (Fig. 2C). Similarly, the ferrous deoxy form of M81A-equivalent iso-1 cyt *c* from yeast has a Soret of 410 nm with a shoulder at 437 nm and peaks at 548 nm with shoulders at 521 and 564 nm (Table S2) (12). The Soret shoulder has been attributed to a mixture of spin states for the chemically synthesized horse heart cyt *c* M81A, whereas the absorbance is consistent with His/OH⁻ ligation state (13). The UV-vis spectrum of our human ferric cyt *c* M81A closely matches the ferric yeast iso-1 cyt *c* variant at pH 7.0 (12).

A spectrum of ferrous cyt *c* H19M (bis-Met) looks similar to WT cyt *c* in its defined α and β maxima (549/520 nm), which is indicative of two strong axial ligands (14). For ferric cyt *c* H19M, a peak is observed at 597 nm, which indicates a penta-coordinate state with one axial ligand (15). No absorbance at 597 nm is observed in the presence of excess imidazole (Fig. S5), consistent with the idea that an open ligand site on heme is now occupied (i.e., the pentacoordinate ferric cyt *c* H19M is hexacoordinate in the presence of imidazole, suggesting a Met/imidazole ligation of ferric iron). Soret maxima of the reduced (425 nm) and oxidized (398.5 nm) are shifted.

There is a prominent shoulder or doublet (418 nm) in the Soret (425 nm) of ferrous cyt *c* H19M (Fig. 2D, Inset). One possible explanation for this doublet is that a heterogeneous population exists with other residues transiently acting as ligands, replacing the methionines. There are two other histidines in cyt *c* H19M, His-27 and His-34, and these have been discussed previously as forming axial ligand intermediates during folding (16, 17). We substituted alanines for H27 and H34 in cyt *c* H19M and WT. No differences were observed in UV-vis spectra of these cyt *c* variants (Fig. S6) and the cyt *c* H19M/H27A/H34A still exhibited the unique doublet in the Soret region of the reduced protein. We determined if the Soret doublet is caused by a titratable group by recording spectra at various pH values (pH 2.6–6.6) (Fig. S7). The only change in the doublet observed was correlated with a change in redox state. Another possibility is that there is a mixture of spin states present with the ferrous iron, as we observe in ferric iron in cyt *c* H19M (see below). We propose that the Soret doublet is a feature of the bis-Met ligation state in the reduced protein.

Electron Paramagnetic Resonance Spectroscopy of cyt *c* Axial Ligand Variants. Electron paramagnetic resonance (EPR) spectroscopy at 10 K was carried out on the oxidized cyt *c* proteins to interrogate the ligand coordination and spin states of the ferric center (Fig. 3). Each cyt *c* exhibits a distinct EPR spectrum, which supports the argument for axial ligand changes in these variants. EPR *g* values less than 4 are typically suggestive of low spin heme centers. In addition the EPR spectra each contain signals at $g = 2.00$ and 2.08 that correspond to organic radical and copper (Cu^{2+}) impurities, respectively, and both signals are marked with an asterisk (*) for all spectra (Fig. 3) (18). The EPR spectrum of WT cyt *c* shows *g* values of 3.09 and 2.19 [g_z value was not detected] which have been noted previously for human cyt *c* (19) and yeast iso-1 cyt *c* (20, 21) (Table S3), and are reflective of the presence of axial His/Met ligands. The EPR of yeast iso-1 cyt *c* has been recorded for Met81 variants: Asp, Ala, Cys, Leu, Lys, Ile, and Phe (21, 22). Of these, yeast iso-1 cyt *c* M81A shows the most similarity to the human cyt *c* M81A signals, which exhibit *g* values at 2.58, 2.18, and 1.86 (Fig. 3). These peaks are representative of the signals that appear for OH⁻ ligation (21) (Table S3). In addition, pronounced peaks are present at 2.08 and 1.97 in human cyt *c* M81A. These are also observed in the yeast iso- cyt *c* M81A variant, albeit with weaker intensity (20, 21). Human cyt *c* M81H exhibits *g* values at 2.91, 2.29, and 1.58, very similar to a cytochrome *b*562 M7H with bis-His ligands to *b* heme and bis-imidazole-ligated hemin (23) (Table S3). We conclude that biosynthesized cyt *c* M81H has bis-His ligation.

Interestingly, the putative bis-Met cyt *c* variant H19M shows the simplest EPR spectra in the low-spin region; there is no

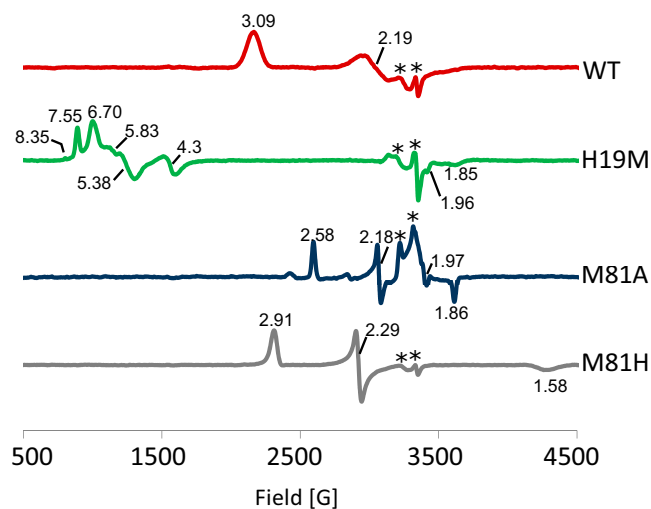


Fig. 3. The EPR spectra of the oxidized cyt *c* variants shows that iron is present in different protein environments. An asterisk (*) denotes signal at $g = 2.00$ or 2.08 , which correspond to organic radical or Cu impurities.

signal with a *g* value near 3, which is necessary for low spin heme and so we conclude that cyt *c* H19M is fully high spin at pH 7.4 (Fig. 3). The high-spin region however has several well-defined peaks (8.35/7.55/6.70, 5.83/5.38/4.30). We attribute these peaks together with the signal at low *g* values (1.96/1.85) to be due to at least two different high-spin heme species that exhibit different degrees of rhombicities. The third, most-rhombic set of signals could be because of a third high-spin heme species, or it could be because of nonheme iron in rhombic coordination (21). These high-spin heme species could have a single Met binding to the iron center and water binding at the opposite axial site. Such a conformation is consistent with the UV-vis ferric cyt *c* H19M spectrum that we observe. When cyt *b*562 axial ligand His102 is changed to methionine, a nearly identical, low-spin signal at 1.98 is exhibited at pH 9.2 (Table S3) (24). Thus, we conclude that the cyt *c* H19M variant possesses Met ligation.

The EPR spectra (Fig. 3) suggest that the least heterogeneity is observed in cyt *c* M81H with only a low-spin species present and a single main set of g_x , g_y , and g_z values. This finding is not surprising because histidine provides the strongest bond to the heme iron center in the proper geometry.

Circular Dichroism Spectroscopy and Thermal Stability of cyt *c* Axial Ligand Variants. Circular dichroism (CD) spectra in the far UV region provides an indication of α -helical composition. CD spectra between 200 and 260 nm of all four cyt *c*'s were identical (Fig. 4A), suggesting that each is folded generally with the same α -helical content. By monitoring secondary structure at 220 nm with temperature increases (Fig. 4B), it is observed that each of the four different axial ligand cyt *c* proteins exhibit a T_m of 90 °C. This is in contrast to the cyt *c* single thioether variants (C15S and C18S), which show significant changes in stability (Fig. 4B). We conclude that regardless of axial ligand changes in cyt *c*, stability and secondary structure are retained, thus likely folding into its native structure.

CD spectra in the near UV Soret region (300–450 nm) probe the immediate heme environment, for example vinyl groups red-shift absorbance and propionates enhance absorption in reconstituted myoglobins (25). Near UV-vis CD spectra of reduced (Fig. 4C) and oxidized (Fig. 4D) cyt *c* proteins show very different absorbance features for each ligand variant, unlike the spectra of WT cyt *c* from different species (26). The WT cyt *c* show typical ellipticities in oxidized and reduced states. All variants are

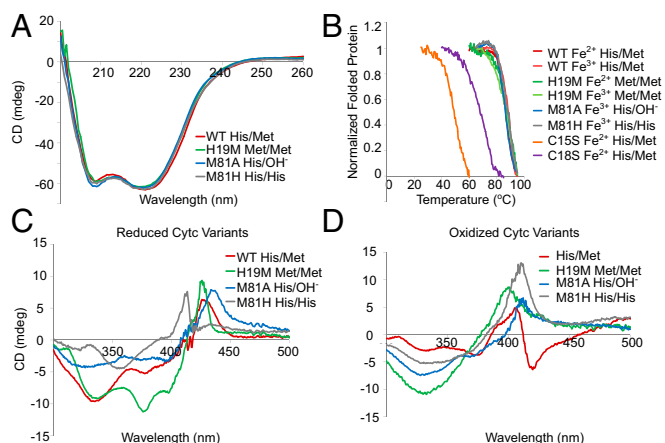


Fig. 4. Secondary structure, thermal stability, and local heme environment analyzed using CD spectroscopy. Indicated are the *cyt c* variant and oxidation state analyzed. (A) The far-UV CD spectrum of *cyt c* WT reduced, H19M reduced, M81A oxidized, M81H oxidized show WT α -helical content. (B) The thermal denaturation of *cyt c* monitoring the secondary structure at 220 nm, shows that the axial ligand variants are similarly stable with $T_m = 90^\circ\text{C}$, in contrast to single thioether variants that show a substantial reduction in stability. (C) The reduced and (D) the oxidized *cyt c* variants show different ellipticity in the near UV region demonstrating unique heme environments.

significantly altered in both positive and negative maxima. In the ferric form of *cyt c*, it has been shown through denaturation with alcohols or binding cardiolipin that the negative ellipticity at 417 nm is a result of Met81 ligation to heme (27, 28). Consistent with this conclusion, *cyt c* M81A and M81H do not exhibit this negative ellipticity (Fig. 4D). *Cyt c* H19M also does not exhibit a negative ellipticity at 417 nm, which might be because of the lack of an Met19 ligand or that Met81 is partially released in the ferric form, as suggested by imidazole effects noted above. CD experiments in the near UV region with oxidized and reduced undecapeptide *cyt c* showed that in the presence of imidazole a bis-His ligation occurs with a peak at 411 nm (29), like the oxidized and reduced *cyt c* M81H recorded here (Fig. 4C and D). The results support conclusions from EPR and UV-vis spectra that each *cyt c* variant has significant ligand differences.

Oxidation/Reduction Potentials of *cyt c* Axial Ligand Variants. Mitochondrial *cyt c* possesses a redox potential of +250 mV, higher than donor *cyt bc₁* but lower than acceptor *cyt a/a₃*. Axial ligand composition is a major factor in the redox potential of a heme or metal protein (30, 31). We determined the redox potentials of the four *cyt c* proteins (Fig. 5; for individual spectra see Fig. S8). As expected, the human WT *cyt c* shows a potential of +252 mV vs. standard hydrogen. The redox potential for *cyt c* M81A (−19 mV) was over 270-mV more negative than WT *cyt c*. A similar potential was determined previously for yeast iso-1-*cyt c* M80A (−80 mV) (20). The potential of *cyt c* M81H (−69 mV) suggests a stabilization of the oxidized cytochrome, similar to the chemically generated horse heart bis-His *cyt c* variant (+41 mV) (11); such a change is often observed when substituting a stronger histidine ligand for methionine. Conversely, substituting a methionine for a histidine ligand is predicted to increase the potential and this is what is observed for *cyt c* H19M (+349 mV), increasing 100 mV over WT *cyt c* (+252 mV). For individual spectra of *cyt c* H19M at each potential (Fig. S8B), we observed that the Soret doublet is maintained throughout the titration but only in the reduced state. This finding again suggests that the doublet is caused by the heme environment and not by the heterogeneity of the ligand state.

Discussion

HCCS Release Mutants. We show that substitutions engineered in conserved residues of HCCS can lead to significant biosynthetic overproduction of unique *cyt c* variants in recombinant *E. coli*. We discuss below how these mutations impact the release step 4 for each *cyt c* variant. We thus term these HCCS “release mutants.” If HCCS release mutants make as much or more *cyt c* than WT HCCS, the question arises as to why these residues are conserved in HCCS (Fig. S1A). We suggest that these residues are necessary for binding heme in step 1 at concentrations of heme present within the mitochondrial intermembrane space. Multiple residues contribute to the heme binding site of HCCS, including heme iron ligand His154 and Glu159, Asn155, and Trp162, all within domain II of HCCS (5). Our data support the hypothesis that in recombinant *E. coli* release of holocyt *c* from HCCS can be increased and release may be a limiting step. We have not tested whether under heme limiting conditions (e.g., iron limitation) the HCCS release mutants become defective in step 1. However, certain release mutants (e.g., W118A) biosynthesize even more WT *cyt c* when heme precursor aminolevulinic acid is added to the culture (5). These data indicate that modulating heme levels as well as using engineered HCCS enzymes can augment biosynthesis. The steps for which each HCCS variant is impacted will depend on the heme levels and potentially other factors in the cell.

Mechanisms of Biosynthesis by HCCS. The bacterial system I and II cytochrome *c* biogenesis pathways are more complex and appear to recognize only the CXXCH motif; thus, no one has engineered them to biosynthesize, for example, bis-Met or single thioether *c*-type cytochromes. The mitochondrial HCCS, on the other hand, recognizes an extended region besides the CXXCH motif, including α -helix 1 immediately preceding CXXCH (32, 33). Recognition of this extended region may help in making new *c*-type cytochromes with substitutions in CXXCH. We showed previously the importance of *cyt c* His19 (of CXXCH) in forming the second axial ligand of the HCCS/*cyt c* complex, with HCCS

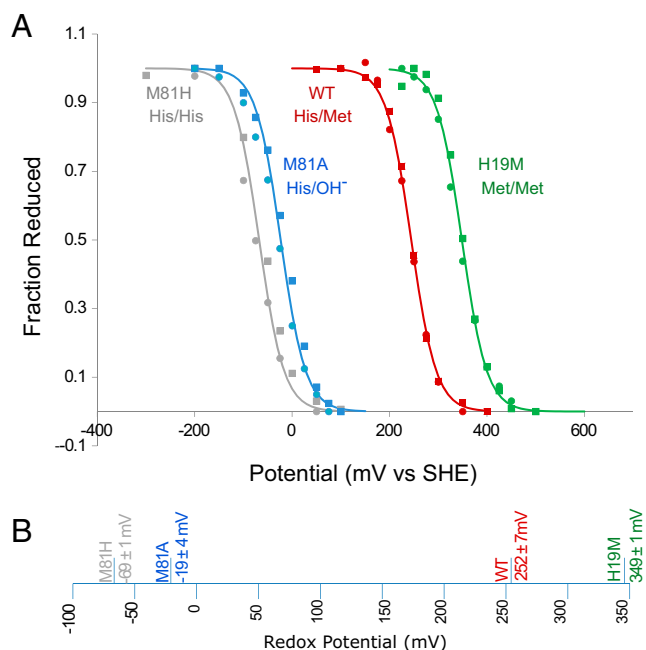


Fig. 5. Redox potentials of *cyt c* wt, H19M, M81A, M81H. (A) The fraction reduced is plotted versus the potential. (B) The redox midpoint potential is plotted to show the range of potentials observed by altering the axial ligation state.

His154 providing the first ligand (Fig. 1, step 2) (4, 6). Only methionine could substitute for cyt *c* His19, whereby Met19 facilitated preparation of the heme for covalent attachment (6). However, the cyt *c* H19M variant was “trapped” in the WT HCCS complex with very low release. We proposed that another role for His19 is to “pull” heme from the HCCS active site. Using HCCS release mutants in putative heme binding residues, we show here that more cyt *c* H19M is released and biosynthesized. This result is consistent with the hypothesis that HCCS must dissociate from heme (as holo-cyt *c*) in its mechanism, and it has evolved a balance in binding (step 1) and release (step 4). Although cyt *c* Met19 is not as strong at “pulling” heme from HCCS, use of the HCCS release mutants counteract this limitation in the biosynthesis of cyt *c* H19M.

HCCS release mutants also facilitate overproduction of certain cyt *c* single thioether variants. The cyt *c* C15S variant has been biosynthesized previously at levels about 10% of WT cyt *c*, using the yeast HCCS (7) or the human HCCS (4). This finding is not too surprising because such single thioether cyt *c*'s (XXXCH) naturally exist in Euglenozoa. Resonance Raman spectroscopy of complexes containing WT HCCS and copurified cyt *c* C15 and C18 variants has provided a possible explanation (6). In the complex with the cyt *c* C15 variant (thioether attached at C18), the heme is more distorted (puckered) than the complex with the cyt *c* C18 variant (thioether attached to C15) (6). We speculated that optimal heme distortion is needed for release from HCCS, thus much less cyt *c* C18S variant is released (less than 3% than that of WT cyt *c*). This hypothesis is supported by results herein, whereby HCCS release mutants increase synthesis of cyt *c* C18 variants up to ninefold over WT HCCS (Table S1), allowing for biosynthesis of this unique single thioether cyt *c*. In this case (C18 variants), release from HCCS is suboptimal because of less heme distortion, thus stronger retention of heme (holo-cyt *c*). Again, weakening the interaction with heme via the HCCS mutations counteracts this defective release.

It is informative that the two cyt *c* variants with defective release properties (cyt *c* H19M and C18A/S) are impacted the most by the use of HCCS release mutations. In this regard, HCCS release mutants appear to have the least effect on overproduction of cyt *c* M81 substitutions, generally providing yields similar to WT HCCS (Table S1). Cyt *c* M81 is proposed to play a role after HCCS-mediated covalent attachment of heme and release, thus after folding begins (Fig. 1). Possibly, this finding explains why HCCS E159A does not impact production levels of at least cyt *c* M81A and M81H.

The cyt *c* Variants Biosynthesized in This Study. We describe biophysical properties of the set of cyt *c* proteins with axial ligand differences (His/Met, Met/Met, Met/OH⁻, His/His), including redox potentials, UV-vis, EPR, and CD analyses, all of which support the axial ligand changes that were engineered. We found that ferric cyt *c* H19M is largely pentacoordinate based on the UV-vis data, together with the addition of imidazole and mostly high-spin species (EPR), whereas the ferrous cyt *c* H19M is hexacoordinate based on UV-vis. Ferrous cyt *c* H19M may also have a mixture of spin states that may explain the doublet in the Soret. For cyt *c* H19M, this ligation state stabilizes the ferrous iron in heme and increases the redox potential by ~100 mV. Studies on denaturation of ferrous cyt *c* have generally agreed that His-19 ligation is extremely stable even under severe conditions (e.g., low pH, guanidine HCl) (34, 35). From this and other studies, one could conclude that the proximal side with His-19 heme ligation is an important initial step in folding. With regards to the involvement of cyt *c* His-19 on folding, biosynthesis of cyt *c* H19M by HCCS suggests that the histidine of CXXCH does not play an essential role in folding at least toward the final native structure. Our results suggest that HCCS release mutants still allow for proper stereochemistry and folding of cyt *c* WT and variants. Future studies using these variants include

continued analysis of unique structural and physical properties, folding kinetics and pathways, as well as their potential interactions in apoptosome formation.

Materials and Methods

Strains and Plasmids and Their Generation. The *E. coli* strain, RK103 (MG1655 Δccm) (10) was cotransformed with a pGEX plasmid (carb^R) containing the human HCCS gene [e.g., pRGK403 (4), HCCS_E159A, HCCS_W118A, HCCS_N155A] (5) and a pBAD plasmid with a human cyt *c* gene (listed in Fig. S9). Mutations were introduced into the pBAD plasmid using site-directed mutagenesis as has been described previously (36).

Bacterial Growth Conditions, Protein Expression, and Purification. *E. coli* strains were grown as previously described (4) and the proteins were expressed overnight. Cyt *c* was isolated as described previously (6). Cyt *c* variants, were purified over 5 mL HiTrap SP-Sepharose. The column was washed with 50 mL of 50 mM Tris pH 8.0 (0 mM, 50 mM, and 75 mM NaCl). The pink cyt *c* was eluted with excess 50 mM Tris pH 8.0, 100 mM NaCl.

Cyt *c* variants with C-terminal cleavable (thrombin cut site, LVPRIGS) hexa-histidine tags were purified over SP-Sepharose resin followed by HisPur cobalt resin (ThermoFisher Scientific). The cyt *c* was eluted from the SP-Sepharose with 50 mM phosphate pH 7.4, 10 mM imidazole, 300 mM NaCl. The eluate was loaded onto 500 μL HisPur Cobalt Resin Slurry, washed with 10-column volumes of wash buffer (50 mM phosphate 7.4, 10 mM imidazole, 300 mM NaCl), and eluted in 50 mM phosphate pH 7.4, 150 mM imidazole, 300 mM NaCl. Excess thrombin was added to the eluate and dialyzed in 8-kD BioDesignDialysis Tubing (ThermoFisher Scientific) overnight at 4 °C in 50 mM Tris pH 8.0, 500 mM NaCl, and 10% (vol/vol) glycerol. The cleaved cytochromes were separated from thrombin and uncleaved product by passage over a mixed HisPur/Benzamidine Sepharose column (GE Healthcare Life Sciences). The cyt *c* was buffer exchanged and concentrated using a Vivaspin Turbo 3-kD centrifugal concentrator (ThermoFisher Scientific).

UV-vis Spectroscopy. UV-vis spectroscopy was recorded on a Shimadzu UV-1800 spectrophotometer at room temperature in 50 mM phosphate buffer pH 7.4. Reduced spectra were recorded with excess sodium dithionite (sodium hydrosulfate). Oxidized spectra were recorded in the presence of excess ammonium persulfate.

EPR Spectroscopy. EPR was performed using a Bruker EMX-PLUS (9.2 GHz) EPR spectrometer at 10 K with quartz sample tubes. Samples were oxidized with excess K₃[Fe(CN)₆] and then desalted with a G25 column (9). The protein sample was concentrated to 3.6 mg/mL in 50:50 (vol/vol) 100 mM sodium phosphate buffer pH 7.4 and glycerol. Four 4-min scans were accumulated and averaged, and the following parameters were used during the collection of the EPR spectra: attenuation, 33 dB; time constant, 0.2 s; modulation amplitude, 1 mT; sweep width, 500 mT; frequency, 9371.852 MHz; power, 0.1 mW.

CD Spectroscopy and Thermal Stability. Equilibrium samples were recorded on a Jasco J-815 at room temperature in 50 mM phosphate buffer pH 7.4, 50 mM NaCl. The machine sensitivity was 100 mdeg, the data pitch was 0.5 nm, the scanning mode was continuous, the scanning speed was 50 nm/min, the response rate 0.5 s for far-UV and 1 s for near-UV, the bandwidth 1 nm, and five accumulations were taken. Thermal stability samples of cyt *c* variants was determined by recording the ellipticity at 220 nm. Temperature was incremented at 0.5 °C/min, absorbance was detected with standard sensitivity, 8-s response time, and a 1-nm bandwidth.

Redox Titrations. Spectroelectrochemistry was performed using a CHI620C CH Instruments potentiostat and a Shimadzu UV-1800 spectrophotometer as described previously (37). Measurements were carried out in 50 mM sodium phosphate buffer (pH 7.0) and 50 mM NaCl. 20 μM each of 4,4-dipyridyl (E° = -0.84 V) (38) and hexamine ruthenium (III) chloride (E° = -0.44 V) were included to mediate electron transfer between the honeycomb and protein in the titrations of cyt *c* M81A and cyt *c* M81H.

Additional methods are described in *SI Materials and Methods*.

ACKNOWLEDGMENTS. We thank Hani Zaher and Kyusik Kim for assistance with the HPLC profiles; Jennifer Hsu for biosynthesis of cyt *c* C18 variants; and Fall 2014 Bio 437 students for the generation of pDLM022 and pDLM023. This work was supported by NIH Grant GM 47909 (to R.G.K.). S.E.B. was supported by NIH National Research Service Award Grant F32GM108278. D.L.M. was a W. M. Keck Fellow for part of this study. The purchase of the Bruker EMX-PLUS EPR spectrometer was supported by the National Science Foundation (MRI, CHE-1429711).

1. Dumont ME, Ernst JF, Hampsey DM, Sherman F (1987) Identification and sequence of the gene encoding cytochrome c heme lyase in the yeast *Saccharomyces cerevisiae*. *EMBO J* 6(1):235–241.
2. Pollock VB, Rosell FI, Twitchett MB, Dumont ME, Mauk AG (1998) Bacterial expression of a mitochondrial cytochrome c. Trimethylation of lys72 in yeast iso-1-cytochrome c and the alkaline conformational transition. *Biochemistry* 37(17):6124–6131.
3. Babbitt SE, Sutherland MC, San Francisco B, Mendez DL, Kranz RG (2015) Mitochondrial cytochrome c biogenesis: No longer an enigma. *Trends Biochem Sci* 40(8):446–455.
4. San Francisco B, Bretsnyder EC, Kranz RG (2013) Human mitochondrial holo-cytochrome c synthase's heme binding, maturation determinants, and complex formation with cytochrome c. *Proc Natl Acad Sci USA* 110(9):E788–E797.
5. Babbitt SE, San Francisco B, Bretsnyder EC, Kranz RG (2014) Conserved residues of the human mitochondrial holo-cytochrome c synthase mediate interactions with heme. *Biochemistry* 53(32):5261–5271.
6. Babbitt SE, et al. (2014) Mechanisms of mitochondrial holo-cytochrome c synthase and the key roles played by cysteines and histidine of the heme attachment site, Cys-XX-Cys-His. *J Biol Chem* 289(42):28795–28807.
7. Rosell FI, Mauk AG (2002) Spectroscopic properties of a mitochondrial cytochrome C with a single thioether bond to the heme prosthetic group. *Biochemistry* 41(24):7811–7818.
8. Silkstone G, Stanway G, Brzezinski P, Wilson MT (2002) Production and characterisation of Met80X mutants of yeast iso-1-cytochrome c: Spectral, photochemical and binding studies on the ferrous derivatives. *Biophys Chem* 98(1-2):65–77.
9. Silkstone G, Stanway G, Wilson MT (1998) Yeast iso-1-cytochrome c met80X mutants: The pKa of the spin state transition as a probe for haem pocket flexibility. *Biochem Soc Trans* 26(4):S348.
10. Feissner RE, et al. (2006) Recombinant cytochromes c biogenesis systems I and II and analysis of haem delivery pathways in *Escherichia coli*. *Mol Microbiol* 60(3):563–577.
11. Raphael AL, Gray HB (1989) Axial ligand replacement in horse heart cytochrome c by semisynthesis. *Proteins* 6(3):338–340.
12. Lu Y, Casimiro DR, Bren KL, Richards JH, Gray HB (1993) Structurally engineered cytochromes with unusual ligand-binding properties: Expression of *Saccharomyces cerevisiae* Met-80→Ala iso-1-cytochrome c. *Proc Natl Acad Sci USA* 90(24):11456–11459.
13. Bren KL, Gray HB (1993) Structurally engineered cytochromes with novel ligand-binding sites—Oxy and carbonmonoxy derivatives of semisynthetic horse heart Ala80 cytochrome-C. *J Am Chem Soc* 115(22):10382–10383.
14. Ran Y, et al. (2007) Bis-methionine ligation to heme iron in the streptococcal cell surface protein Shp facilitates rapid heme transfer to HtsA of the HtsABC transporter. *J Biol Chem* 282(43):31380–31388.
15. Ran Y, et al. (2010) Spectroscopic identification of heme axial ligands in HtsA that are involved in heme acquisition by *Streptococcus pyogenes*. *Biochemistry* 49(13):2834–2842.
16. Colón W, Wakem LP, Sherman F, Roder H (1997) Identification of the predominant non-native histidine ligand in unfolded cytochrome c. *Biochemistry* 36(41):12535–12541.
17. Hagen SJ, Latypov RF, Dolgikh DA, Roder H (2002) Rapid intrachain binding of histidine-26 and histidine-33 to heme in unfolded ferrocycytochrome C. *Biochemistry* 41(4):1372–1380.
18. Zoppellaro G, et al. (2008) Modulation of the ligand-field anisotropy in a series of ferric low-spin cytochrome c mutants derived from *Pseudomonas aeruginosa* cytochrome c-551 and *Nitrosomonas europaea* cytochrome c-552: A nuclear magnetic resonance and electron paramagnetic resonance study. *J Am Chem Soc* 130(46):15348–15360.
19. Rajagopal BS, et al. (2013) The hydrogen-peroxide-induced radical behaviour in human cytochrome c-phospholipid complexes: Implications for the enhanced pro-apoptotic activity of the G41S mutant. *Biochem J* 456(3):441–452.
20. Amacher JF, et al. (2015) A compact structure of cytochrome c trapped in a lysine-ligated state: Loop refolding and functional implications of a conformational switch. *J Am Chem Soc* 137(26):8435–8449.
21. Silkstone GG, Cooper CE, Svistunenko D, Wilson MT (2005) EPR and optical spectroscopic studies of Met80X mutants of yeast ferricytochrome c. Models for intermediates in the alkaline transition. *J Am Chem Soc* 127(1):92–99.
22. Zhong F, Lisi GP, Collins DP, Dawson JH, Pletneva EV (2014) Redox-dependent stability, protonation, and reactivity of cysteine-bound heme proteins. *Proc Natl Acad Sci USA* 111(3):E306–E315.
23. Hay S, Wydrzynski T (2005) Conversion of the *Escherichia coli* cytochrome b562 to an archetype cytochrome b: a mutant with bis-histidine ligation of heme iron. *Biochemistry* 44(1):431–439.
24. Barker PD, et al. (1996) Bis-methionine ligation to heme iron in mutants of cytochrome b562. 1. Spectroscopic and electrochemical characterization of the electronic properties. *Biochemistry* 35(42):13618–13626.
25. Nagai M, Nagai Y, Imai K, Neya S (2014) Circular dichroism of hemoglobin and myoglobin. *Chirality* 26(9):438–442.
26. Vinogradov S, Zand R (1968) Circular dichroism studies. I. Cytochrome c. *Arch Biochem Biophys* 125(3):902–910.
27. Birk AV, et al. (2013) The mitochondrial-targeted compound SS-31 re-energizes ischemic mitochondria by interacting with cardiolipin. *J Am Soc Nephrol* 24(8):1250–1261.
28. Kaminsky LS, Yong FC, King TE (1972) Circular dichroism studies of the perturbations of cytochrome c by alcohols. *J Biol Chem* 247(5):1354–1359.
29. Urry DW (1967) Model systems for interacting heme moieties. I. The heme undecapeptide of cytochrome c. *J Am Chem Soc* 89(16):4190–4196.
30. Tezcan FA, Winkler JR, Gray HB (1998) Effects of ligation and folding on reduction potentials of heme proteins. *J Am Chem Soc* 120(51):13383–13388.
31. Reedy CJ, Elvekrog MM, Gibney BR (2008) Development of a heme protein structure-electrochemical function database. *Nucleic Acids Res* 36(Database issue):D307–D313.
32. Babbitt SE, Hsu J, Kranz RG (2016) Molecular basis behind inability of mitochondrial holo-cytochrome c synthase to mature bacterial cytochromes: Defining a critical role for cytochrome c α helix-1. *J Biol Chem* 291(34):17523–17534.
33. Kleingardner JG, Bren KL (2011) Comparing substrate specificity between cytochrome c maturation and cytochrome c heme lyase systems for cytochrome c biogenesis. *Metallomics* 3(4):396–403.
34. Droghetti E, Oellerich S, Hildebrandt P, Smulevich G (2006) Heme coordination states of unfolded ferrous cytochrome C. *Biophys J* 91(8):3022–3031.
35. Santoni E, et al. (2004) A model for the misfolded bis-His intermediate of cytochrome c: The 1-56 N-fragment. *J Inorg Biochem* 98(6):1067–1077.
36. Mendez DL, Mandt RE, Elgin SC (2013) Heterochromatin Protein 1a (HP1a) partner specificity is determined by critical amino acids in the chromo shadow domain and C-terminal extension. *J Biol Chem* 288(31):22315–22323.
37. King JD, et al. (2013) Metalloproteins diversified: The araucyanins are a family of cupredoxins that stretch the spectral and redox limits of blue copper proteins. *Biochemistry* 52(46):8267–8275.
38. Krishnan CV, Creutz C, Schwarz HA, Sutin N (1983) Reduction potentials for 2,2'-bipyridine and 1,10-phenanthroline couples in aqueous-solutions. *J Am Chem Soc* 105(17):5617–5623.
39. Romão CV, et al. (2000) A bacterioferritin from the strict anaerobe *Desulfovibrio sulfuricans* ATCC 27774. *Biochemistry* 39(23):6841–6849.
40. Kellog JA, Bren KL (2002) Characterization of recombinant horse cytochrome c synthesized with the assistance of *Escherichia coli* cytochrome c maturation factors. *Biochim Biophys Acta* 1601(2):215–221.
41. Brautigan DL, et al. (1977) Multiple low spin forms of the cytochrome c ferrihemo-chrome. EPR spectra of various eukaryotic and prokaryotic cytochromes c. *J Biol Biochem* 252(2):574–582.
42. Zoppellaro G, et al. (2006) Low-temperature EPR and Mössbauer spectroscopy of two cytochromes with His-Met axial coordination exhibiting HALS signals. *J Inorg Chemphyschem* 7(6):1258–1267.
43. Bertini I, Luchinat C, Piccoli M, Soriano A (1998) Folding properties of iron-sulfur proteins. *Inorg Chem Acta* 238:12–16.
44. Cheesman MR, et al. (1997) Two enzymes with a common function but different heme ligands in the forms as isolated. Optical and magnetic properties of the heme groups in the oxidized forms of nitrite reductase, cytochrome cd1, from *Pseudomonas stutzeri* and *Thiosphaera pantotropha*. *Biochemistry* 36(51):16267–16276.
45. van Wonderen JH, et al. (2007) Activation of the cytochrome cd1 nitrite reductase from *Paracoccus pantotrophus*. Reaction of oxidized enzyme with substrate drives a ligand switch at heme c. *J Biol Chem* 282(38):28207–28215.
46. Cheesman MR, et al. (1992) E.p.r. and magnetic circular dichroism spectroscopic characterization of bacterioferritin from *Pseudomonas aeruginosa* and *Azotobacter vinelandii*. *Biochem J* 286(Pt. 2):361–367.